ARTICLE
PUBLISHED ONLINE: 12 JUNE 2011 | DOI: 10.1038/NCHEMBIO.585

A biosensor generated via high-throughput screening quantifies cell edge Src dynamics

Akash Gulyani[1,4], Eric Vitriol[1,4], Richard Allen[1], Jianrong Wu[1], Dmitriy Gremyachinskiy[1], Steven Lewis[2], Brian Dewar[1], Lee M Graves[1], Brian K Kay[3], Brian Kuhlman[2], Tim Elston[1] & Klaus M Hahn[1]*

Fluorescent biosensors for living cells currently require laborious optimization and a unique design for each target. They are limited by the availability of naturally occurring ligands with appropriate target specificity. Here we describe a biosensor based on an engineered fibronectin monobody scaffold that can be tailored to bind different targets via high-throughput screening. We made this Src-family kinase (SFK) biosensor by derivatizing a monobody specific for activated SFKs with a bright dye whose fluorescence increases upon target binding. We identified sites for dye attachment and changes to eliminate vesiculation in living cells, providing a generalizable scaffold for biosensor production. This approach minimizes cell perturbation because it senses endogenous, unmodified target, and because sensitivity is enhanced by direct dye excitation. Automated correlation of cell velocities and SFK activity revealed that SFKs are activated specifically during protrusion. Activity correlates with velocity, and peaks 1–2 μm from the leading edge.

Signaling networks that control cell behavior are tightly regulated in space and time. Fluorescent biosensors for living cells have provided a valuable window on the dynamics of these networks, enabling quantification of the kinetics and localization of protein activity *in vivo*. However, their application has been limited because they remain difficult to design, requiring considerable optimization for each target and identification of 'affinity reagents' that bind a specific state of the targeted protein (for example, phosphorylation or conformation). Biosensors generate a fluorescence readout through attachment of fluorophores at positions unique to each biosensor, so they require extensive optimization. Here we demonstrate that a biosensor can be based on a fixed, engineered scaffold whose binding can be tailored to different target proteins via high-throughput screening. By using a uniform scaffold, with only a small variable region to confer specificity, it is possible to greatly simplify optimization of fluorescence readout mechanisms such as FRET or attachment of environmentally sensitive dyes. Furthermore, high-throughput screening can provide biosensors when no naturally occurring affinity reagents are known.

In the application described here, we chose to detect binding of the monobody to its target by attaching a bright, environmentally sensitive fluorescent dye to the monobody. Binding of the biosensor to endogenous target protein generates a change in fluorescence intensity and/or λ_{max} of the attached dye. We have previously described use of a dye-labeled protein domain to sense an endogenous target with dyes designed for this purpose[1–4]. The dyes can be excited at >580 nm to minimize cell damage and avoid cellular autofluorescence, and they are very bright in hydrophobic environments (quantum yield = 0.17–0.61 and ε > 100,000). This approach minimizes cell perturbation both because it detects endogenous, unaltered target protein and because a bright dye is directly excited, requiring lower concentrations of biosensor. Here we use the biosensor to study SFKs at the thin leading edge of motile cells, where sensitivity and the ability to use low biosensor concentrations are important.

We selected the fibronectin (FN3) monobody[5] as the scaffold that will be the basis of the new biosensor because it is small (~95 residues), it folds stably within living cells, and the invariable portion need not have cysteines (simplifying dye attachment and folding in the reducing environment of the cell)[5]. This monobody, derived from the tenth type III domain of human FN3, has an immunoglobulin-like fold composed of seven β-strands connected by flexible loops. Several of these flexible loops can be randomized while the core structure is kept intact[5–8], thereby creating libraries of 10^9–10^{11} variants. FN3 libraries have been screened by phage display[8] and other methods to produce binders of a variety of targets[5–7]. All these features make the FN3 domain an attractive candidate for a generalizable live-cell biosensor scaffold (**Fig. 1a**).

SFKs are regulators of signaling networks affecting cell division, migration and survival[9,10]. Because they modulate multiple pathways, their activation must be tightly regulated. SFK stimulation via different cell-surface receptors, including integrins[11] and receptor tyrosine kinases[12], activates SFKs in distinct subcellular locations, with tightly controlled kinetics. A biosensor that enabled visualization of SFK activity would be valuable in analyzing the coordinated regulation of these different pathways. Existing biosensors reveal the phosphorylation of Src substrates[13–15], but no studies of Src in protrusion and retraction dynamics at the cell's leading edge have been reported, probably because signal-to-noise considerations limit quantitative studies in this region of the cell. We show that the new biosensor provides the sensitivity required for quantitative studies of protrusion and retraction dynamics. Furthermore, it is advantageous that the new biosensor reports SFK conformation, rather than phosphorylation of a substrate liable to diffusion and susceptible to both kinases and phosphatases.

Below we characterize a monobody that binds the SFKs, demonstrating that it is specific for the activated, 'open' conformation of these kinases. We tested dyes at different positions around the monobody binding interface, identifying sites where attachment provides good fluorescence response without interfering with target

[1]Department of Pharmacology, University of North Carolina at Chapel Hill, Chapel Hill, North Carolina, USA. [2]Department of Biochemistry and Biophysics, University of North Carolina at Chapel Hill, Chapel Hill, North Carolina, USA. [3]Department of Biological Sciences, University of Illinois at Chicago, Chicago, Illinois, USA. [4]These authors contributed equally to this work. *e-mail: khahn@med.unc.edu

binding. Structure-activity studies together with modeling provided insights into the interactions of the dyes with the monobody and target that may be useful in applying the merobody to other targets. The merobody was engineered to eliminate vesiculation in living cells and to include a fluorescent protein for ratio imaging. Within cells, robust detection of SFK activity at the leading edge, combined with quantitative analysis, reveals changing dynamics correlated with protrusion and retraction velocity.

RESULTS

The monobody binds active SFKs without kinase inhibition

The monobody biosensor described here is based on monobody 1F11, which has been shown to bind selectively to the SH3 domains of SFKs and contains no cysteines[6]. 1F11 was generated by phage-display screening using the SH3 domain of Src as 'bait'. It binds to SFKs, but not to closely related kinases[6]. Because it was screened against the SH3 domain, we surmised that this monobody might be conformationally sensitive. Crystallography and biochemical data indicate that the Src SH3 may be more exposed upon Src activation (**Fig. 1b**). Upon activation, two intramolecular linkages are broken to produce a more 'open' conformation, enabling autophosphorylation that maintains the active conformation[16].

We first tested whether 1F11 is specific for the open, activated conformation of Src. In pull-down assays, we examined binding of 1F11 to Src in lysates from GN4 rat liver epithelial cells (**Fig. 2a**,**b**). These cells show robust Src activation when treated with the small molecule ciglitazone[17,18]. 1F11 or wild-type FN3 monobody (nonbinding control) were immobilized on nickel–nitrilotriacetic acid beads and incubated with cell lysates, then tested for the ability to pull down endogenous Src. Total levels of Src were unaffected by this treatment[17] (**Supplementary Results**, **Supplementary Fig. 1**). The 1F11 monobody pulled down substantially more Src from ciglitazone-treated cells than from untreated cells, indicating preferential binding to activated kinase (**Fig. 2a** and **Supplementary Fig. 2**). Wild-type FN3 domain or beads alone showed no Src binding. We have shown previously that pretreatment of GN4 cells with the phosphatase inhibitor pervanadate prevents ciglitazone-mediated Src activation by blocking dephosphorylation of pTyr529 (refs. 17,18). Here we found that pretreatment with pervanadate greatly attenuated 1F11 pull-down of Src (**Fig. 2a** and **Supplementary Fig. 2**). Therefore, our data indicate that pull-down is indeed sensitive to Src activation state.

In vitro kinase assays showed that the SFKs pulled down by the biosensor were active (**Fig. 2b**). This indicated that biosensor binding to the target would not block the kinase activity of SFKs. 1F11 beads that had been incubated with ciglitazone-treated lysates showed kinase activity several-fold higher than wild-type FN3 beads, control beads or 1F11 beads incubated with untreated lysates (**Fig. 2b**). Together, these studies showed that 1F11 binds preferentially to the active form of Src, that 1F11 does not artificially activate the kinase and that Src remains an active kinase when bound to 1F11.

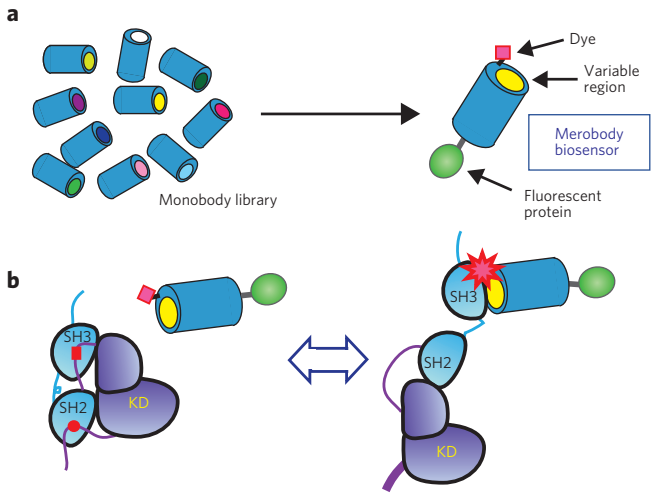

Figure 1 | Screening an FN3 monobody library leads to a biosensor for Src family activity. (**a**) A library of FN3 monobodies is screened to find a library member with the appropriate binding selectivity and affinity for the targeted protein state. The library is based on a uniform scaffold stable in living cells and suitable for conversion to biosensors. The appropriate library member is fused to a fluorescent protein (FP) via a flexible linker and further derivatized with an environmentally sensitive dye to report target binding. (**b**) The present biosensor is based on a binder that is specific for the activated conformation of SFKs. Biosensor binding to active SFKs leads to increased fluorescence from the merocyanine dye. The ratio of dye fluorescence to protein fluorescence provides a quantitative measure of SFK activation kinetics and localization in living cells.

Optimizing affinity, brightness and fluorescence change

Four solvent-sensitive merocyanine dyes were screened at four positions near the variable loops of the monobody. Single-cysteine mutants of the 1F11 monobody fused to monomeric cerulean fluorescent protein (mCerulean)[19] were expressed in *E. coli* and covalently derivatized with dyes bearing cysteine-reactive iodoacetamide side chains[2,4]. These were selected from a set of highly fluorescent fluorophores (**Fig. 3a**) described previously, optimized for use as part of biosensors in living cells[2–4]. The mCerulean was included for ratio imaging *in vivo*, as explained below. Covalent dye-protein conjugates were separated from free dye by size-exclusion chromatography. Dye/protein molar ratios were between 0.8 and 1.1 in all cases, and controls using cysteine-free protein produced dye/protein ratios <0.05. Polyacrylamide electrophoresis gels, which separate protein from unreactive free dye, indicated there was no detectable free dye in the labeled proteins.

The four sites selected for dye attachment were on or near the putative binding interface. This interface comprises residues on the BC and FG loops of 1F11, including those that were randomized for SH3 binding[6]. Three of the dye attachment sites (52, 53 and 55) were on the DE loop adjacent to the BC and FP loops, proximal to the binding interface (**Fig. 3b**). The fourth site, Ala24, is part of the BC binding loop but is not among the residues that were randomized for phage-display screening. This Ala24 site was selected because it would be proximal to the putative binding interface but less likely to disrupt SH3 binding. Each dye conjugate was evaluated for fluorescence change in response to recombinant c-Src SH3, as well as for brightness in the bound and unbound states (**Fig. 3**).

Of all the variations tested, three showed substantial response: dye mero87 at position 53 (C53-m87), dye mero53 at position 52 (C52-m53) and dye mero53 at position 24 (C53-m24) (**Fig. 3c**). At least for this target, the two closely related dyes mero87 and mero53 showed far stronger responses than other structures, albeit at different positions. These two dyes differ only in the positioning of the sulfate group used to confer water solubility on the dye. The Discussion describes modeling of dye-protein interactions and more detailed analysis. Control biosensors lacking a crucial proline residue in the FG binding loop of 1F11 (P78A) showed no response to SH3, for all three of the well-responding variants (**Fig. 3d** and data not shown).

The three biosensors that showed substantial response to Src SH3 were titrated with the SH3 to examine whether sequence modification or dye attachment affected the monobody's affinity for the SH3 domain (**Fig. 3d** and **Supplementary Fig. 3**). The apparent binding constants for C53-m87, C52-m53 and C24-m53 were 0.97, 0.26 and 0.69 μM, respectively, compared to 0.25 μM for the native 1F11 monobody (as measured by isothermal titration calorimetry[6]). The dye-labeled, binding-incompetent P78A mutant of

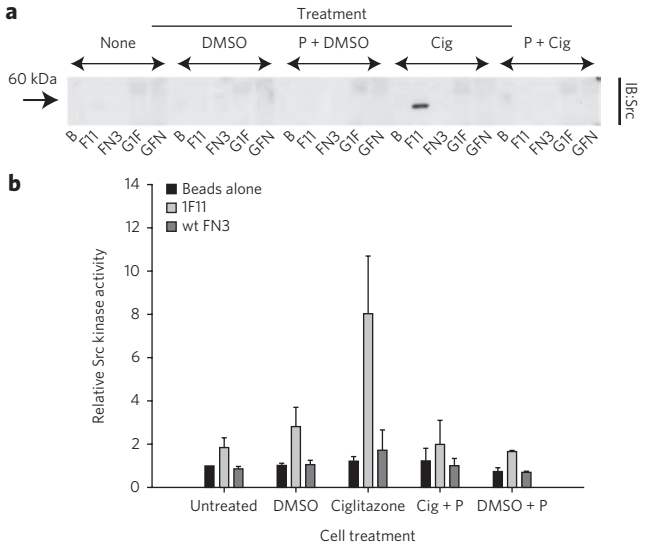

Figure 2 | Fibronectin monobody 1F11 preferentially binds active Src. (**a**) 1F11 monobody binding to Src in lysates from cells with or without the Src activator ciglitazone. GN4 cells were either untreated or treated with vehicle DMSO, vehicle plus pervanadate pretreatment (P), 50 μM ciglitazone (Cig) or ciglitazone with pervanadate pretreatment. Immunoblotting was used to assay pull-down of Src by beads alone (B), the 1F11 monobody (1F11), a control nonbinding monobody (WT FN3), GFP-1F11 with suboptimal linker (G1F) or GFP-FN3 sub-optimal linker (GFN). (**b**) Src kinase activity bound to the monobody or controls as in **a**. Data shown are averages of three independent experiments.

the monobody showed no affinity for the SH3 in these assays. These data showed that labeling 1F11 with merocyanine dyes and fusing it to mCerulean minimally perturbed target binding.

Biosensor C24-mero53 was selected for live-cell studies, and it is referred to simply as the SFK merobody biosensor henceforth. Although this biosensor did not undergo the greatest change in response to SH3 binding, its 50% increase was nonetheless substantial and compares favorably with many biosensors that have proven valuable *in vivo*[14,20,21]. This biosensor was selected because it remained extremely bright when the dye was attached to the monobody. Even in aqueous environments before target binding, the dye emission was greater than that of the mCerulean on the biosensor (**Supplementary Fig. 4** and **Supplementary Table 1**), and upon target binding, dye emission increased to ~2.4-fold that of cerulean. Usefulness in living cells is a function of both dynamic range and brightness. A dye with impressive fluorescence change can be too dim to discern at nonperturbing biosensor concentrations *in vivo*.

Optimizing the fibronectin scaffold for living cells

Initial studies in cells showed that the dye-conjugated native monobody had problems that made it unsuitable for live-cell imaging. Although the 1F11 monobody conjugated to mero87 showed a response to SH3 domain *in vitro* (**Supplementary Fig. 5**), it showed extensive vesiculation in living cells (**Supplementary Fig. 6**). This has been observed previously with dye-labeled proteins (data not shown) and is probably due to autophagy[22] or proteolytic processing[23]. For use of the FN3 monobody as a broadly applicable scaffold for biosensors, it is crucial to eliminate this vesiculation, as fluorescent puncta hinder quantification *in vivo* and could obscure real interactions with punctate cell structures. To examine whether this problem was caused by the dye or the merobody structure, we conjugated 1F11 at the same position to commercially available Alexa 488, a water-soluble dye used frequently to generate fluorescent protein conjugates for live-cell imaging[24]. This conjugate also showed vesiculated and non-uniform distribution in cells (**Supplementary Fig. 6**). We concluded that further modification of the FN3 monobody would be required before it could be used as a biosensor.

The monobody was fused to green fluorescent protein (GFP) and GFP variants in an attempt to enhance solubility or alter the balance of charges that might contribute to autophagy. This also provided a second fluorophore for ratiometric imaging of dyes that responded to SFKs by changing their fluorescence intensity; the ratio of dye fluorescence to fluorescent protein fluorescence could be used to normalize out effects of cell thickness, uneven illumination and other external influences on dye brightness[1,25,26]. GFP variants without surface-exposed cysteines were prepared so that cysteine labeling could still be used for site-specific dye incorporation. The fluorescent protein was attached to the N terminus, as our earlier studies had shown that attachment at the C terminus interfered with SH3 interactions (data not shown). Attachment of GFP did eliminate the vesiculation, but to our surprise, it also completely abrogated the fluorescence response of the dye (**Supplementary Fig. 7**). Increasing the length of the linker between the monobody and the fluorescent protein (**Supplementary Fig. 8**) restored fluorescence response without eliminating the uniform monobody distribution in cells (**Supplementary Fig. 6**). The distribution of fluorescence appeared the same both at the dye wavelengths and at the wavelengths of the fluorescent protein, indicating that the puncta were not simply concentrations of free dye. In the final, optimized monobody, mCerulean with a C48S mutation (to prevent dye labeling) was attached to the N terminus of 1F11.

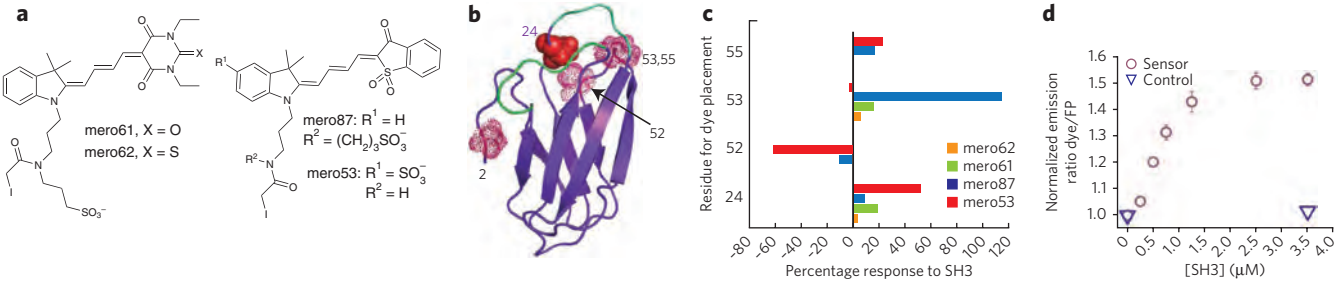

Figure 3 | Screening for responsive sensor variants, selecting dye and site for dye labeling. (**a**) Structures of the environmentally sensitive merocyanine dyes tested on the monobody. (**b**) Ribbon representation of the active-state binder 1F11 (based on published FN3 domain crystal structure PDB 1FNA). Residues 2, 24, 52, 53 and 55, where cysteine was incorporated for dye attachment and testing, are shown as space-filling side chains. Ala24, labeled in red, marks the position of dye attachment in the final merobody biosensor. The putative target-binding loops are shown in cyan. (**c**) Ratiometric fluorescence response (dye emission/mCerulean emission) of the various combinations of mero dyes and residues labeled. (**d**) Titration showing how the normalized emission ratio of mero53/mCerulean for the biosensor or control (0.5 μM) changes with increasing c-Src SH3. The control sensor has a P80A mutation in the FG binding loop of 1F11.

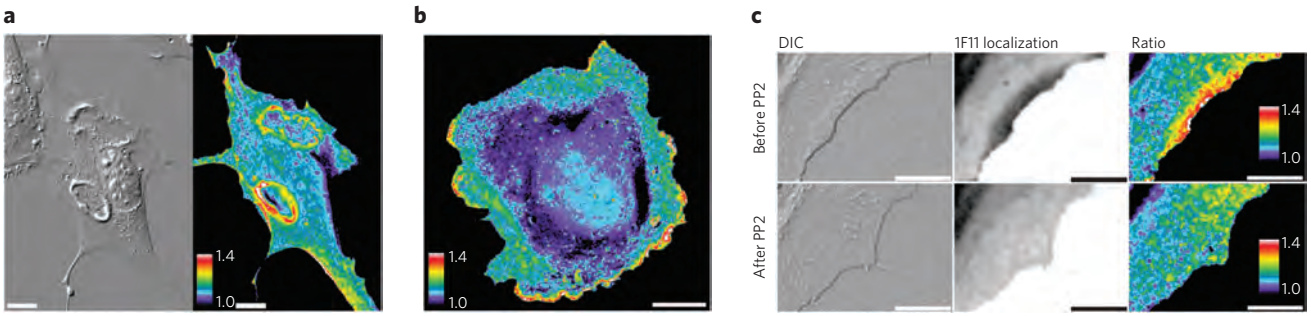

Figure 4 | Src activation dynamics in living cells. (**a**) Differential interference contrast (DIC) image (left) and ratio image (right) of a PDGF-stimulated NIH 3T3 MEF microinjected with the SFK merobody biosensor. Scale bar, 20 μm. Note prominent circular dorsal ruffles. (**b**) Ratio image of a PTK1 cell microinjected with the biosensor. Scale bar, 20 μm. (**c**) DIC (left), mCerulean (merobody localization, middle) and ratio images (right) from representative frames of a movie in which a PTK1 cell microinjected with the biosensor was treated with the Src inhibitor PP2 (**Supplementary Videos 4–6**). Scale bar, 10 μm.

Spatio-temporal dynamics of SFK activity in motile cells

Although Src family members have been clearly implicated in motility, analysis of their dynamics within protrusions and retractions has not been reported, perhaps owing to the difficulty of obtaining sufficient signal within the thin cell edge. We first applied the SFK monobody biosensor in NIH 3T3 mouse embryo fibroblasts (MEFs). Ratio imaging and cell handling were as previously described[1,25], with SFK activity indicated by an increase in the dye/cerulean emission ratio.

During initial studies, SFK activity was observed at the edges of extending protrusions and in dorsal ruffles (large, circular, actin-based protrusions). We stimulated MEFs with platelet-derived growth factor (PDGF)[27,28] to induce dorsal ruffling and cell protrusions and to verify the previous finding of Src activation there. Immunostaining has shown that Src is specifically localized within dorsal ruffles[29] and at the cell edge[28–31]. Also, Src activity is thought to be necessary for ruffle formation and cell protrusion[28,29]. The merobody showed elevated SFK activity within the ruffles from the time of their appearance until they closed to become macropinosomes (**Fig. 4a**, **Supplementary Video 1** and **Supplementary Fig. 9**). Closure was accompanied by a sudden drop in activation. These experiments directly demonstrated that Src is activated within ruffles specifically during periods of ruffle formation and movement, as would be expected given Src's role in regulating actin polymerization[27].

We next focused our attention on protrusion and retraction at the cell edge, where velocity could more readily be quantified, enabling detailed correlation of SFK activity with specific aspects of cell movement (**Supplementary Video 2**). SFKs are probably involved in controlling both actin and adhesion dynamics[9,10,28,32–34]. A more detailed understanding of SFK dynamics during extension and retraction could help to differentiate potential roles and mechanisms. By titrating down the amount of biosensor in cells (roughly determined as brightness per unit area, an appropriate measure for the flat cells used) we were able to define brightness ranges with good signal-to-noise ratios where there was no apparent perturbation of extension and protrusion. Controls indicated that, at the biosensor concentrations we used, the velocities of protrusion and retraction were not correlated with the amount of biosensor present in the cell (**Supplementary Fig. 10**). There was no visible difference in cell-edge dynamics between cells injected with the SFK monobody, noninjected cells or cells injected with P78A control biosensor incapable of binding Src.

For quantification of protrusion and retraction dynamics, we switched to PTK1 kangaroo-rat kidney epithelial cells because of their large, flat lamellipodia. During constitutive protrusion, we discovered a band of high SFK activity immediately adjacent to the cell edge (**Fig. 4b,c**; also see **Supplementary Videos 3** and **4** and **Supplementary Fig. 11**). We also observed that the biosensor itself localized to the cell edge in protrusions, as detected by monitoring mCerulean fluorescence (**Fig. 4c** and **Supplementary Video 4**). This indicated a substantial enrichment of active SFKs along the edge. The nonbinding control biosensor P78A showed no change in fluorescence ratio (**Supplementary Fig. 12**) and no cell-edge enrichment. The specificity of 1F11 for different SH3 domains was examined extensively in the original paper describing the 1F11 monobody[6], but we confirmed specificity for SFKs in living cells by examining the effect of the Src kinase inhibitor PP2. PP2 abolished both high fluorescence ratios and localization of the probe to the cell edge within 3 min after PP2 addition (**Fig. 4c** and **Supplementary Videos 4–6**).

To quantify the relationship between SFK dynamics and protrusion or retraction, we correlated the distribution of SFK activity with edge velocity. Briefly, our automated approach first involved tracking the cell edge and deriving the velocity at each pixel along the cell boundary. This was based on methods described elsewhere[35,36]. From a given pixel at the edge, we generated 'line scans' by bi-linearly interpolating pixel values along vectors oriented into the cell and normal to the edge (**Supplementary Fig. 13**). For every pixel along the edge of the cell and for each time point, there was a line scan and an edge velocity. Line-scan values were calculated for 1 μm from the edge to 20 μm into the cell. The first portion of the line scan (0–1 μm) was found to be subject to a lower signal-to-noise ratio in both fluorescence channels, potentially leading to artifacts in the ratio image. We therefore excluded from our analysis regions within 1 μm of the edge. The portion of the line scan 1–20 μm from the cell edge was sufficient to clearly delineate regions of SFK activation and differences between protrusion and retraction. The line scans were sorted by velocity into bins of width 0.2 pixels per frame. Then, for each cell and each velocity bin, a mean line scan was calculated.

Figure 5 shows the average SFK activity as a function of distance from the cell edge during protrusion. SFK activity peaked between 1 and 2 μm from the cell edge, with a gradual decline of activity at points further into the cell. This activation was greatly diminished when the control monobody incapable of target binding (P78A) was used, or when cells were treated with PP2. The distribution of SFK activity was dependent on the velocity and direction of edge movement. **Figure 5b** shows the correlation of cell-edge velocity and the SFK activity profile. With a total of 270,460 line scans for the merobody biosensor, the data indicated that SFK activation is greater during protrusion than retraction, that activation level is proportional to the velocity of the protrusion, and that the distribution of activity relative to the cell edge is consistently highest at a single peak 1–2 μm from the edge (for both retraction and protrusion). The control biosensor (266,623 line scans) again showed greatly reduced activity (**Fig. 5d**), and the Src inhibitor PP2 (145,240 line scans before treatment and 138,320 scans after treatment) flattened the activity profile (**Supplementary Fig. 14**). Furthermore, edge velocity gradually decreased after addition of PP2 (**Supplementary Fig. 15**).

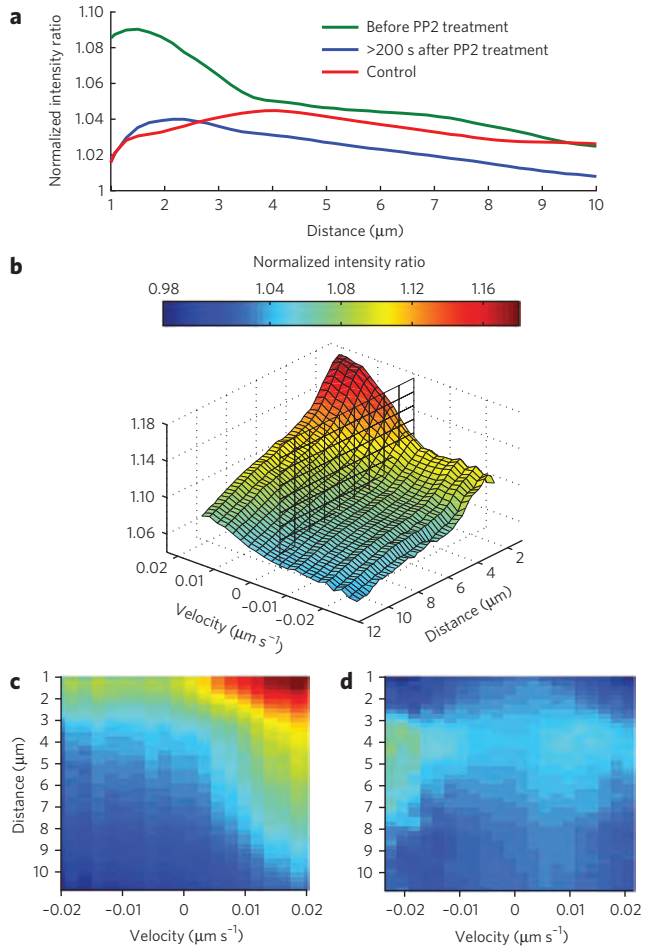

Figure 5 | Automated edge analysis and line scans reveal a distinct zone of SFK activity that is correlated with protrusion velocity. (**a**) SFK activity as a function of distance (μm) from the cell edge. SFK activity is localized toward the edge of the cell and is inhibited by PP2 treatment. For all data points, the s.e.m. is less than 0.1%. At 1 μm, the difference between the mean normalized intensity ratio, before and after PP2 treatment, is ~0.08 and is statistically significant ($P < 0.001$). (**b**) SFK activity as a function of distance from the cell edge and velocity. SFK activity is approximately proportional to protrusion speed. The vertical plane is at velocity = 0. The s.e.m., for a given velocity and distance, is less than 0.3%. (**c**,**d**) Response of the merobody biosensor (**c**) compared to the nonbinding control (**d**). The merobody biosensor reports both higher activity than the nonbinding control and a stronger dependence on velocity. The s.e.m. for a given velocity and distance is less than 0.3% (**c**) and less than 1% (**d**).

DISCUSSION

The goal of these studies was a biosensor based on an engineered scaffold designed for high-throughput screening. This proof-of-principle study paves the way for generating other biosensors via screening, for targets where no suitable naturally occurring binders are known, and for greatly simplifying biosensor engineering. To study Src-family signaling at the cell's leading edge, we based this prototype biosensor on a known FN3 monobody that binds specifically to the SH3 domains of SFKs[6]. The FN3 monobody was a good choice for a generally applicable biosensor scaffold because it contains no native cysteines (facilitating site-specific dye attachment) and folds well in living cells. This contrasts with scFv and other antibody fragments[37]. The FN3 monobody has flexible loops that accommodate insertion and randomization of amino acid residues, and it has proven capacity to generate binders of diverse protein targets[5,6,38]. We used a solvent-sensitive merocyanine dye to report target binding, which provided enhanced sensitivity, with brightness more than twice that from direct excitation of cerulean fluorescent protein and therefore substantially brighter than fluorescent proteins indirectly excited for FRET. This proved valuable at the thin edge of cells, where signal-to-noise is an important limitation. This biosensor design could report activation of endogenous target protein, thereby reducing cell perturbation.

We showed that the monobody had the desired specificity for active SFKs, and we then examined where dyes could be attached around the binding site to report target binding without greatly diminishing affinity. Three different sites were suitable, indicating that dyes will probably be able to provide readouts for monobodies binding to different proteins. The four fluorophores tested were designed for use in living cells: they were bright ($\varepsilon > 100{,}000$, QY = 0.17–0.61 in hydrophobic environments), with excitation at ≥550 nm to avoid autofluorescence and minimize cell damage, and they had solvent-sensitive fluorescence suitable for reporting protein binding *in vivo*[2,4].

Notably, for the two dyes based on the coupled indolenine and benzothiophen-3-one-1,1-dioxide rings (mero87 and mero53), shifting the position of attachment determined whether the dye showed an increase or decrease of fluorescence upon target binding. The attachment site producing a decrease in fluorescence (position 52) is positioned at the interface between the β-sheet and the flexible DE loop. Dye attachment may have caused partial unfolding of the monobody, allowing the dye to bind a hydrophobic pocket in the monobody before interaction with target protein. Binding to the target could force the dye out of the pocket, thereby decreasing fluorescence. This would be driven partially by restoration of binding interactions that stabilize the monobody. For positions and dyes showing an increase in emission intensity upon binding (C53-m87 and C24-m53), the dye probably experienced a more hydrophobic environment upon target binding. Although dye mero87 at position 53 gave the largest response (**Fig. 3**), its low overall brightness on the monobody led us to select dye mero53 at position 24 for use in living cells. This dye showed a 50% fluorescence increase upon target binding and was 2.4 times as bright as cerulean fluorescent protein. The labeled monobody had 500–600 nM affinity for Src SH3, a range proven valuable for biosensor reversibility and specificity in previous studies[1,21,39].

We generated computer models of 1F11-mero53 conjugates and docked these models to Src SH3 to examine the merobody-target interface (**Fig. 6** and **Supplementary Figs. 16** and **17**). With the biosensor used for live-cell studies, our modeling suggests that the dye does not directly interact with the SH3 domain. Rather, it experiences a change in local environment owing to differing interactions with the FN3 monobody itself (**Fig. 6a**). Modeling suggests that the water-exposed surface area of the dye decreases as the merobody binds the target SH3 (**Fig. 6b**,**c**), consistent with the observed increase in dye emission upon binding. Merocyanine dyes, including mero53, generally have greater emission intensity when shifting from polar to apolar environments. The decrease in solvent-accessible surface area (see **Fig. 6c**) is, in fact, more pronounced for the specific moiety on the merocyanine (the sulfone) that is believed to confer sensitivity to solvent polarity[2]. The models do not show changes in solvation for mero53 attached at positions that produced poor fluorescence response (**Supplementary Figs. 16** and **17**).

Finally, we attached a fluorescent protein via an optimized linker to eliminate the formation of fluorescent puncta, possibly owing to autophagy, which would have severely hindered live-cell imaging. We are hopeful that these changes, and the identification of optimum dye-attachment sites, have generated a scaffold that can now be targeted to other intracellular proteins, providing a generalizable tool to study endogenous protein conformation. This work has demonstrated the feasibility of generating practical biosensors from engineered

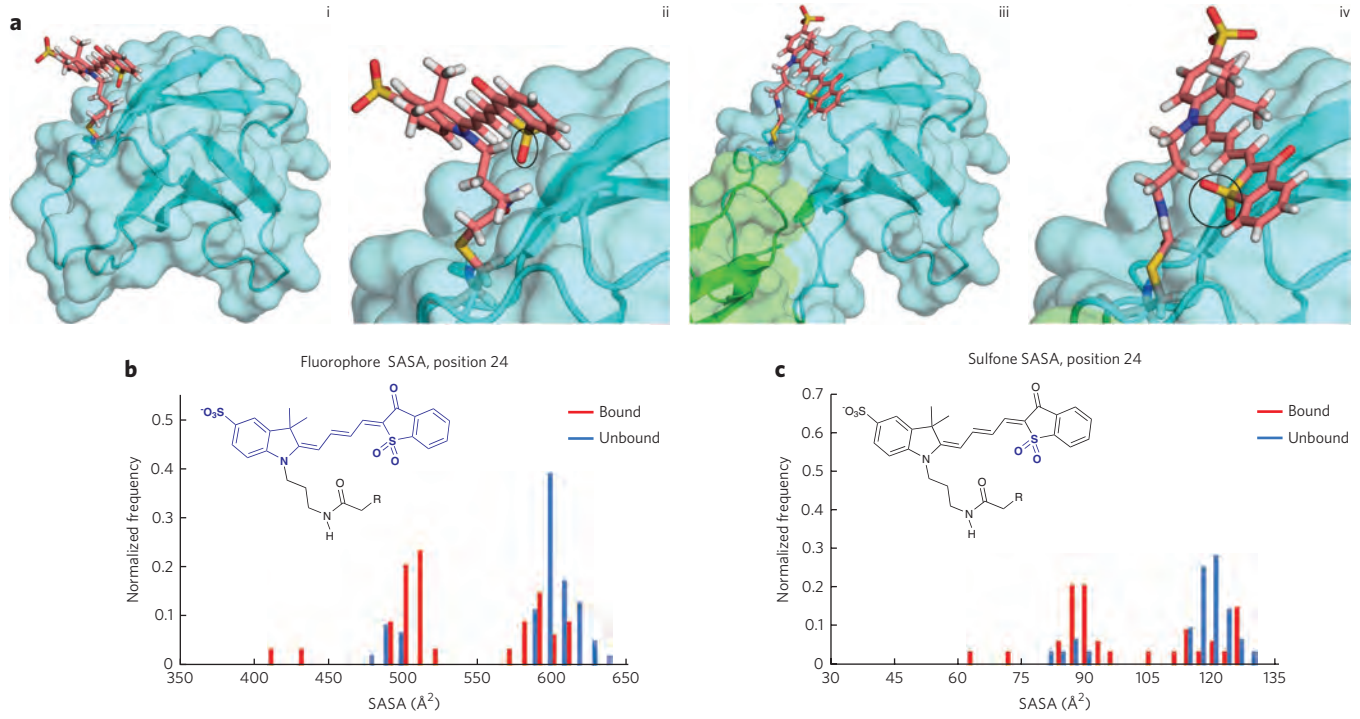

Figure 6 | Modeling of the 1F11 dye–SH3 interface. (**a**) Computer models of either unbound 1F11-mero53 conjugate alone (i and ii) or 1F11-mero53 in complex with cSrc-SH3 (iii and iv). Dye is attached to residue 24, as in the final 'merobody' biosensor. c-Src SH3 is green, 1F11 is blue and dye is salmon. In (ii) and (iv) (magnified versions), the sulfone group of the dye is circled. The model of unbound biosensor shown here is part of the subpopulation in which the dye has higher solvent-accessible surface area (SASA). The model of bound biosensor is the highest-scoring model and a member of the low-SASA cluster. (**b**,**c**) SASA distribution for the top 0.5% of models of the bound and unbound states, either for the whole fluorophore (**b**) or the sulfone group (**c**).

scaffolds. It is important to note that essentially all biosensors perturb cell physiology, as they must interact with the molecules whose behaviors they report. Different designs either inhibit or mimic normal protein action. The SFK monobody biosensor described here may compete with endogenous ligands that normally bind to the SH3 domain of Src-family proteins. This could either generate 'false negative' data, in which native ligands outcompete biosensor, or the biosensor could inhibit normal interactions. The enhanced sensitivity of the SFK merobody will enable us to use less biosensor, more closely approaching the equilibria in unperturbed cells.

The SFK monobody revealed localized and transient activation of SFKs at the cell edge and in PDGF-induced dorsal ruffles. Immunostaining has shown that phosphorylated, active Src localizes to dorsal ruffles and at the cell edge[28–31], where it phosphorylates cortactin or N-WASP, leading to activation of Arp2/3 and consequent actin polymerization[27,40–42]. Src is known to be necessary for the formation of dorsal ruffles, and SFKs are known to regulate signaling molecules involved in actin assembly and organization within these ruffles[27] (Abl tyrosine kinase[43], Rac GTPase[44]). The merobody biosensor provided direct evidence, consistent with these previous studies, that endogenous SFKs are in the active conformation within ruffles specifically during actin-based protrusion.

The biosensor was used to study SFK activation in the lamellipodia of migrating cells. Through development of a quantitative line-scanning approach, we were able to obtain statistically valid correlations of protrusion velocity and Src activity distribution based on thousands of line scans. Though it was elevated in both protrusion and retraction, SFK activity was substantially higher during cell protrusion. Most notably, during protrusion the activity was proportional to the rate of lamellipodial extension. SFK activity may regulate protrusion speed by controlling the rate and extent of actin polymerization, potentially through phosphorylation of actin-regulatory proteins (possibly the WAVE complex[40,41], cortactin[40,45], gelsolin, pCAS[46,47], Abl tyrosine kinase[29,43] or regulators of Rho family GTPases[12,34,44,48–50]). The biosensor showed that activation occurred with a defined profile, peaking within 2 μm of the edge in the lamellipodium of the PTK1 cells. Src kinases are crucial in regulating both actin dynamics and the assembly and disassembly of adhesions[33,34,47], so SFKs at this position may regulate actin, focal adhesions or their coordination. Further work will be required to define the interactions of SFKs with specific molecules at the leading edge, and their positions relative to actin and adhesion dynamics. SFK activation in retraction is much less pronounced and may be part of constitutive signaling responsible for edge retraction[48].

In conclusion, we have demonstrated that it is feasible to produce a biosensor based on modification of the FN3 monobody, a scaffold suitable for high-throughput screening and for use in living cells. This exemplifies a generalizable approach capable of producing biosensors when no suitable affinity reagents are known, to increase the throughput of biosensor production and to greatly simplify biosensor design. These biosensors report the activation of endogenous, unmodified proteins, thereby reducing perturbation of cell physiology. The dyes used here provided exceptional sensitivity, but made it more difficult to introduce the biosensor into living cells. Ultimately, it may be possible to use fluorescent proteins for genetically encoded readouts of endogenous target binding. Automated image analysis revealed that SFKs are more strongly activated during protrusion than retraction and that the level of activity is proportional to the velocity of the extending edge. Automated analysis of multiple points along the cell edge revealed an activity profile with a single peak of maximal activation at the edge of constitutively migrating PTK cells.

METHODS

Dye labeling. DMSO solutions of cysteine-reactive merocyanine dyes (10–20 mM) were added to 1F11-mCerulean fusion proteins (200–300 μM) in 50 mM

HEPES buffer with 100 mM NaCl pH 7.4, so that the dye was present in five- to ten-fold molar excess and the DMSO in the reaction mixture was less than 10% (v/v). After reaction for 4–5 h, excess dye was separated from labeled protein using size-exclusion G-25 (GE healthcare) columns. During G-25 size exclusion, a clear separation was seen between the labeled protein band and the relatively immobile free dye. Labeled proteins were subjected to SDS-PAGE electrophoresis, and a single fluorescent band was observed (controls in which labeled monobody and dye were mixed showed that free dye could be observed as a separate band of lower molecular weight). Coomassie labeling was also used to verify homogeneity of the biosensor preparations. Labeling efficiency was calculated by measuring the dye and protein concentrations of the labeled conjugate. Dye concentration was estimated using dye absorbance at absorption maxima after dissolving the conjugate in DMSO. Protein concentration was estimated by using absorbance due to the mCerulean (molar extinction coefficient 43,000). Labeling efficiency was estimated to be in the range of 0.9–1.2 dye/protein molar ratio, for the various preparations tested. Binding to SH3 was compared for individual batches, and similar results were obtained. Also, independent batches gave consistent results in live-cell imaging experiments.

Microscopy. For imaging experiments, MEFs and PTK1 cells were plated onto coverslips coated with 5 μg ml^{-1} fibronectin (Sigma) overnight. Culture media was exchanged for imaging media for 1 h before microinjection. Cells were micro-injected using a biosensor concentration of 40 μM in the microinjection needle and were allowed to recover for 30–60 min before imaging experiments. MEFs were stimulated using 30 ng ml^{-1} PDGF (Sigma). For inhibition of SFKs, PTK1 cells were treated with 10 μM PP2 (Sigma).

Automated line-scanning and analysis of Src activity. The response of the biosensor was analyzed using custom automated line-scanning software. Line scans of length 100 pixels (~20 μm) were calculated at every pixel around the edge of the cell and oriented into the cell in a direction normal to the edge. For each line scan, we assigned a velocity by using the previous frame to calculate the velocity of cell edge at that location (see **Supplementary Methods**). Line scans were then grouped, and averaged, by velocity (**Fig. 6**).

Additional methods. Cell culture, biosensor design and construct generation, protein expression and purification, pulldown and *in vitro* kinase experiments, dye labeling, binding assays, microscopy, automated line-scanning and analysis of Src activity, and modeling of dye on the 1F11/SH3 interface are described in the **Supplementary Methods**.

Received 12 October 2010; accepted 19 April 2011; published online 12 June 2011; corrected online 15 June 2012

References

1. Nalbant, P., Hodgson, L., Kraynov, V., Toutchkine, A. & Hahn, K.M. Activation of endogenous Cdc42 visualized in living cells. *Science* **305**, 1615–1619 (2004).
2. Toutchkine, A., Kraynov, V. & Hahn, K. Solvent-sensitive dyes to report protein conformational changes in living cells. *J. Am. Chem. Soc.* **125**, 4132–4145 (2003).
3. Toutchkine, A., Nguyen, D.V. & Hahn, K.M. Merocyanine dyes with improved photostability. *Org. Lett.* **9**, 2775–2777 (2007).
4. Toutchkine, A., Nguyen, D.V. & Hahn, K.M. Simple one-pot preparation of water-soluble, cysteine-reactive cyanine and merocyanine dyes for biological imaging. *Bioconjug. Chem.* **18**, 1344–1348 (2007).
5. Koide, A., Bailey, C.W., Huang, X. & Koide, S. The fibronectin type III domain as a scaffold for novel binding proteins. *J. Mol. Biol.* **284**, 1141–1151 (1998).
6. Karatan, E. *et al.* Molecular recognition properties of FN3 monobodies that bind the Src SH3 domain. *Chem. Biol.* **11**, 835–844 (2004).
7. Koide, A., Abbatiello, S., Rothgery, L. & Koide, S. Probing protein conformational changes in living cells by using designer binding proteins: application to the estrogen receptor. *Proc. Natl. Acad. Sci. USA* **99**, 1253–1258 (2002).
8. Sidhu, S.S. & Koide, S. Phage display for engineering and analyzing protein interaction interfaces. *Curr. Opin. Struct. Biol.* **17**, 481–487 (2007).
9. Parsons, S.J. & Parsons, J.T. Src family kinases, key regulators of signal transduction. *Oncogene* **23**, 7906–7909 (2004).
10. Thomas, S.M. & Brugge, J.S. Cellular functions regulated by Src family kinases. *Annu. Rev. Cell Dev. Biol.* **13**, 513–609 (1997).
11. Playford, M.P. & Schaller, M.D. The interplay between Src and integrins in normal and tumor biology. *Oncogene* **23**, 7928–7946 (2004).
12. Bromann, P.A., Korkaya, H. & Courtneidge, S.A. The interplay between Src family kinases and receptor tyrosine kinases. *Oncogene* **23**, 7957–7968 (2004).
13. Ouyang, M., Sun, J., Chien, S. & Wang, Y. Determination of hierarchical relationship of Src and Rac at subcellular locations with FRET biosensors. *Proc. Natl. Acad. Sci. USA* **105**, 14353–14358 (2008).
14. Wang, Y. *et al.* Visualizing the mechanical activation of Src. *Nature* **434**, 1040–1045 (2005).
15. Ting, A.Y., Kain, K.H., Klemke, R.L. & Tsien, R.Y. Genetically encoded fluorescent reporters of protein tyrosine kinase activities in living cells. *Proc. Natl. Acad. Sci. USA* **98**, 15003–15008 (2001).
16. Cowan-Jacob, S.W. *et al.* The crystal structure of a c-Src complex in an active conformation suggests possible steps in c-Src activation. *Structure* **13**, 861–871 (2005).
17. Gardner, O.S., Dewar, B.J., Earp, H.S., Samet, J.M. & Graves, L.M. Dependence of peroxisome proliferator-activated receptor ligand-induced mitogen-activated protein kinase signaling on epidermal growth factor receptor transactivation. *J. Biol. Chem.* **278**, 46261–46269 (2003).
18. Dewar, B.J. *et al.* Capacitative calcium entry contributes to the differential transactivation of the epidermal growth factor receptor in response to thiazolidinediones. *Mol. Pharmacol.* **72**, 1146–1156 (2007).
19. Rizzo, M.A., Springer, G.H., Granada, B. & Piston, D.W. An improved cyan fluorescent protein variant useful for FRET. *Nat. Biotechnol.* **22**, 445–449 (2004).
20. Fosbrink, M., Aye-Han, N.N., Cheong, R., Levchenko, A. & Zhang, J. Visualization of JNK activity dynamics with a genetically encoded fluorescent biosensor. *Proc. Natl. Acad. Sci. USA* **107**, 5459–5464 (2010).
21. Pertz, O., Hodgson, L., Klemke, R.L. & Hahn, K.M. Spatiotemporal dynamics of RhoA activity in migrating cells. *Nature* **440**, 1069–1072 (2006).
22. Glick, D., Barth, S. & Macleod, K.F. Autophagy: cellular and molecular mechanisms. *J. Pathol.* **221**, 3–12 (2010).
23. Reis, R.C., Sorgine, M.H. & Coelho-Sampaio, T. A novel methodology for the investigation of intracellular proteolytic processing in intact cells. *Eur. J. Cell Biol.* **75**, 192–197 (1998).
24. Panchuk-Voloshina, N. *et al.* Alexa dyes, a series of new fluorescent dyes that yield exceptionally bright, photostable conjugates. *J. Histochem. Cytochem.* **47**, 1179–1188 (1999).
25. Hodgson, L., Shen, F. & Hahn, K. Biosensors for characterizing the dynamics of rho family GTPases in living cells. *Curr. Protoc. Cell Biol.* **46**, 14.11.1–14.11.26 (2010).
26. Bright, G.R., Fisher, G.W., Rogowska, J. & Taylor, D.L. Fluorescence ratio imaging microscopy. *Methods Cell Biol.* **30**, 157–192 (1989).
27. Buccione, R., Orth, J.D. & McNiven, M.A. Foot and mouth: podosomes, invadopodia and circular dorsal ruffles. *Nat. Rev. Mol. Cell Biol.* **5**, 647–657 (2004).
28. Veracini, L. *et al.* Two functionally distinct pools of Src kinases for PDGF receptor signalling. *Biochem. Soc. Trans.* **33**, 1313–1315 (2005).
29. Veracini, L. *et al.* Two distinct pools of Src family tyrosine kinases regulate PDGF-induced DNA synthesis and actin dorsal ruffles. *J. Cell Sci.* **119**, 2921–2934 (2006).
30. Sandilands, E., Brunton, V.G. & Frame, M.C. The membrane targeting and spatial activation of Src, Yes and Fyn is influenced by palmitoylation and distinct RhoB/RhoD endosome requirements. *J. Cell Sci.* **120**, 2555–2564 (2007).
31. Sandilands, E. *et al.* RhoB and actin polymerization coordinate Src activation with endosome-mediated delivery to the membrane. *Dev. Cell* **7**, 855–869 (2004).
32. Cary, L.A., Klinghoffer, R.A., Sachsenmaier, C. & Cooper, J.A. SRC catalytic but not scaffolding function is needed for integrin-regulated tyrosine phosphorylation, cell migration, and cell spreading. *Mol. Cell. Biol.* **22**, 2427–2440 (2002).
33. Fincham, V.J. & Frame, M.C. The catalytic activity of Src is dispensable for translocation to focal adhesions but controls the turnover of these structures during cell motility. *EMBO J.* **17**, 81–92 (1998).
34. Frame, M.C., Fincham, V.J., Carragher, N.O. & Wyke, J.A. v-Src's hold over actin and cell adhesions. *Nat. Rev. Mol. Cell Biol.* **3**, 233–245 (2002).
35. Machacek, M. & Danuser, G. Morphodynamic profiling of protrusion phenotypes. *Biophys. J.* **90**, 1439–1452 (2006).
36. Machacek, M. *et al.* Coordination of Rho GTPase activities during cell protrusion. *Nature* **461**, 99–103 (2009).
37. Renard, M. *et al.* Knowledge-based design of reagentless fluorescent biosensors from recombinant antibodies. *J. Mol. Biol.* **318**, 429–442 (2002).
38. Koide, A., Jordan, M.R., Horner, S.R., Batori, V. & Koide, S. Stabilization of a fibronectin type III domain by the removal of unfavorable electrostatic interactions on the protein surface. *Biochemistry* **40**, 10326–10333 (2001).
39. Kraynov, V.S. *et al.* Localized Rac activation dynamics visualized in living cells. *Science* **290**, 333–337 (2000).
40. Martinez-Quiles, N., Ho, H.Y., Kirschner, M.W., Ramesh, N. & Geha, R.S. Erk/Src phosphorylation of cortactin acts as a switch on-switch off mechanism that controls its ability to activate N-WASP. *Mol. Cell. Biol.* **24**, 5269–5280 (2004).
41. Cory, G.O., Garg, R., Cramer, R. & Ridley, A.J. Phosphorylation of tyrosine 291 enhances the ability of WASp to stimulate actin polymerization and filopodium formation. Wiskott-Aldrich Syndrome protein. *J. Biol. Chem.* **277**, 45115–45121 (2002).
42. Suetsugu, S. *et al.* Sustained activation of N-WASP through phosphorylation is essential for neurite extension. *Dev. Cell* **3**, 645–658 (2002).

43. Plattner, R., Kadlec, L., DeMali, K.A., Kazlauskas, A. & Pendergast, A.M. c-Abl is activated by growth factors and Src family kinases and has a role in the cellular response to PDGF. *Genes Dev.* **13**, 2400–2411 (1999).
44. Sini, P., Cannas, A., Koleske, A.J., Di Fiore, P.P. & Scita, G. Abl-dependent tyrosine phosphorylation of Sos-1 mediates growth-factor-induced Rac activation. *Nat. Cell Biol.* **6**, 268–274 (2004).
45. Yang, L., Kowalski, J.R., Zhan, X., Thomas, S.M. & Luscinskas, F.W. Endothelial cell cortactin phosphorylation by Src contributes to polymorphonuclear leukocyte transmigration in vitro. *Circ. Res.* **98**, 394–402 (2006).
46. Bouton, A.H., Riggins, R.B. & Bruce-Staskal, P.J. Functions of the adapter protein Cas: signal convergence and the determination of cellular responses. *Oncogene* **20**, 6448–6458 (2001).
47. Polte, T.R. & Hanks, S.K. Complexes of focal adhesion kinase (FAK) and Crk-associated substrate (p130(Cas)) are elevated in cytoskeleton-associated fractions following adhesion and Src transformation. Requirements for Src kinase activity and FAK proline-rich motifs. *J. Biol. Chem.* **272**, 5501–5509 (1997).
48. DerMardirossian, C., Rocklin, G., Seo, J.Y. & Bokoch, G.M. Phosphorylation of RhoGDI by Src regulates Rho GTPase binding and cytosol-membrane cycling. *Mol. Biol. Cell* **17**, 4760–4768 (2006).
49. Timpson, P., Jones, G.E., Frame, M.C. & Brunton, V.G. Coordination of cell polarization and migration by the Rho family GTPases requires Src tyrosine kinase activity. *Curr. Biol.* **11**, 1836–1846 (2001).
50. Rossman, K.L., Der, C.J. & Sondek, J. GEF means go: turning on RHO GTPases with guanine nucleotide-exchange factors. *Nat. Rev. Mol. Cell Biol.* **6**, 167–180 (2005).

Acknowledgments

We thank C. MacNevin for assistance with dye synthesis, F. Shen for help with imaging studies, D. Renfrew for assistance with computational modeling, A. Nguyen for technical assistance and B. Clarke for administrative assistance. We gratefully acknowledge funding from the American Heart Association (A.G.) and the US National Institutes of Health (GM GM082288 and GM057464 to K.M.H.).

Author contributions

A.G. developed the biosensors, with help from B.D. and L.M.G. on phosphorylation assays. E.V. carried out live-cell imaging studies, assisted by A.G. R.A. and T.E. developed the image analysis algorithms and carried out automated analysis of SFK activity, with help from J.W. S.L. and B.K. modeled dye-protein interactions. D.G. synthesized the dyes. B.K.K. provided protein constructs and input regarding FN3 screening and structure. K.M.H. conceived the study, directed the research and wrote the final manuscript based on contributions from all authors.

Competing financial interests

The authors declare no competing financial interests.

Additional information

Supplementary information is available online at http://www.nature.com/naturechemicalbiology/. Reprints and permissions information is available online at http://www.nature.com/reprints/index.html. Correspondence and requests for materials should be addressed to K.M.H.

CORRIGENDUM

A biosensor generated via high-throughput screening quantifies cell edge Src dynamics

Akash Gulyani, Eric Vitriol, Richard Allen, Jianrong Wu, Dmitriy Gremyachinskiy, Steven Lewis, Brian Dewar, Lee M Graves, Brian K Kay, Brian Kuhlman, Tim Elston & Klaus M Hahn

Nat. Chem. Biol. **7**, 437–444 (2011); published online 12 June 2011; corrected after print 15 June 2012

In the version of this article initially published, the residue numbers indicated in the *y*-axis labels in Figure 3c were incorrectly written as 24, 53, 55 and 53 from the origin but should have read 24, 52, 53 and 55. The error has been corrected for the PDF and HTML versions of this article.